Proceedings World Geothermal Congress 2000
Kyushu - Tohoku, Japan, May 28 - June 10, 2000

ESTIMATION OF STRESS FIELD BY USING DRILLING-INDUCED TENSILE FRACTURES OBSERVED AT WELL TG-2 AND A STUDY OF CRITICALLY STRESSED SHEAR FRACTURES BASED ON THE STRESS FIELD

Takashi Okabe[1] and Kazuo Hayashi[2]
[1] Geothermal Energy Research and Development Co., Ltd., Kyodo Bldg., 11-7, Kabuto-cho, Nihonbashi, Chuo-ku, Tokyo 103-0026, Japan
[2] Institute of Fluid Science, Tohoku University, Katahira 2-1-1, Aoba-ku, Sendai 980-8577, Japan

Keywords: Stress field, Drilling-induced tensile fracture, BHTV/FMI, Inversion, TG-2, Critically stressed shear fractures

ABSTRACT

We have proposed a new method to estimate *in situ* three-dimensional stress fields using data from drilling-induced tensile fractures (DTFs) observed in a single inclined borehole (Okabe et al., 1998). A DTF is a longitudinal crack consisting of many small parallel cracks which are oblique to the borehole axis. A DTF is characterized by its circumferential position (θ_{mD}) along the borehole surface and the inclination (γ_m) of the small cracks with respect to the borehole axis. Based on the variation of θ_{mD} and γ_m as functions of borehole orientation which changes with depth, an inverse problem is formulated to estimate the three-dimensional stress field.

We have previously applied this method to well TG-2 located in the northern area of Japan and have estimated the stress field. In the case of TG-2, thermal stresses may be significant since TG-2 is located in the rim of the Matsukawa geothermal field. However, because we did not account for the effects of thermal stresses, only relative stress magnitudes were determined. We recently included thermal stresses and have performed the inversion again. In this paper, we discuss the results and study critically stressed shear fractures observed in the FMI log, using the estimated stress field to investigate the feasibility of identifying permeable fractures. The stress field interpreted by the data from borehole TG-2 shows that the averaged directions of the principal axes of stress are N 45.7° W ± 9.0°, 13.9° NW ± 6.0° for σ_1 (the maximum compressive principal stress), N 51.0 °E ± 11.4°, 20.1° SW ± 4.6° for σ_2 (the intermediate compressive principal stress) and S 14.1° W ± 8.1°, 64.5° SE ± 5.2° for σ_3 (the minimum compressive principal stress) and the magnitudes of σ_1, σ_2 and σ_3 are 22.7 MPa ± 1.4, 16.4 MPa ± 0.6 and 12.4 MPa ± 0.5, respectively. All three principal stresses have been determined with reasonable certainty. The three stress directions from the result agree with the previous result for the case without consideration of thermal stresses and direction of σ_1 obtained from the inversion agrees with that obtained by the stress relief method at a nearby field. Interpretation of critically stressed shear fractures based on the stress field derived above shows that there are not many fractures stressed critically. Stresses normal to the bedding planes are mostly orientated to σ_3 and it is possible that fluid flows through the bedding planes while injection PTS (Pressure/Temperature/Spinner) logging. Interpreted critically stressed shear fractures are approximately NS～EW strikes and low dip angle. The strikes agree with those of the three faults estimated in the Matsukawa geothermal field.

1. INTRODUCTION

Evaluation of *in situ* three-dimensional stress fields is conducted not only for tunnel excavations and earthquake prediction projects but also for estimating the direction of fracture propagation during hydraulic fracturing. Hydraulic fracturing techniques are used for enhancement of oil and gas recovery and creation of geothermal heat extraction systems such as HDR (Hot Dry Rock) and HWR (Hot Wet Rock) systems which utilize hydraulically stimulated fractures as fluid flow paths for heat exchange (Abé and Hayashi, 1992). The stress state in the earth's crust is one of the main factors that controls the growth behavior of fractures during hydraulic stimulation. Among a number of methods developed to measure stress in the earth's crust, the hydraulic fracturing stress measurement method (e.g., Haimson,1988) is most promising for depths greater than a few thousand meters. In the course of the HWR Project of NEDO (the New Energy and Industrial Technology Development Organization of Japan), we found fractures, induced during drilling, by FMI (formation micro imager) and/or BHTV (borehole televiewer) logging in borehole TG-2. Hereafter we call these fractures "drilling-induced tensile fractures" (DTF). These fractures consist of many small inclined fractures which are parallel to each other and make up, as a whole, two longitudinal fractures which are parallel to the borehole axis macroscopically (Fig. 1). Obviously, DTF is created due to the stress concentration of *in situ* regional stresses, pressure of drilling mud and thermal stresses due to the cooling of the borehole surface. Thus, the circumferential position of the macroscopic longitudinal fractures and the inclination of small fractures have certain explicit relationships with *in situ* stresses. Therefore, it seems to be possible to estimate *in situ* stress state by using DTF data in principle. The advantage of such an approach is that we do not need any special operations such as hydraulic stimulation under severe conditions since DTF is formed just by drilling boreholes. We only have to measure the circumferential position and inclination of small fractures of DTF detected by FMI or BHTV after drilling. The mechanism of the formation of DTF is exactly the same as that of fracture formation during hydraulic fracturing. Namely, the circumferential position is the position at which the tensile stress induced by the three-dimensional stress concentration on the borehole surface takes a maximum value. The small cracks are normal to the maximum tensile stress at the circumferential position just mentioned. There are theoretical studies (Hayashi et al., 1985; Daneshy, 1973; Yew and Li, 1988) on DTF and also there are studies (e.g., Aadnoy, 1990; Peška and Zoback, 1995) examining the feasibility of estimating the *in situ* regional stress state by using the information of DTF obtained in an inclined borehole. We recently have developed a direct inversion technique for evaluating *in situ* regional stress state by using the information (Okabe et al., 1998). Stress field is one of the main factors that effect permeability. We investigated if critically stressed shear fractures calculated from the stress field are permeable, based on the previous study (Barton et al., 1995).

The objective of the present paper is to analyze DTF data, i.e., the macroscopic circumferential position and the inclination of small fractures of DTF, obtained in TG-2 including consideration of thermal stresses in order to estimate stress field and to interpret critically stressed shear fractures based on the calculated stress field.

2. METHOD TO ESTIMATE STRESS FIELD

We use three coordinate systems to describe the stress state on the borehole wall (Fig. 2). The Cartesian coordinate system (x, y, z) is used for describing the far-field stress components σ_x, σ_y, σ_z, τ_{xy}, τ_{yz} and τ_{zx}, where the far-field stress state means the stress state existing before drilling. The coordinate system (x′, y′, z′) is the supplementary Cartesian coordinate system, where the z′-axis coincides with the borehole axis (ζ). The cylindrical coordinate system (r, θ, ζ) describes

the stress state on the borehole wall. The far-field stress components referred to the coordinate system (x′, y′, z′) are denoted by $\sigma_{x'}$, $\sigma_{y'}$, $\sigma_{z'}$, $\tau_{x'y'}$, $\tau_{y'z'}$ and $\tau_{z'x'}$. Hydrostatic pressure due to drilling mud and thermal stresses developed while drilling is denoted by P_w and P_t, respectively. The stress components referred to in the cylindrical coordinate system (r, θ, ζ) are denoted by σ_r, σ_θ, σ_ζ, $\tau_{r\theta}$, $\tau_{\theta\zeta}$ and $\tau_{\zeta r}$. Tensile stresses are taken to be positive. The following relation holds on the borehole wall (Hiramatsu and Oka, 1961).

$$\left.\begin{aligned}
&\sigma_r = -P_w,\\
&\sigma_\theta = \sigma_{x'} + \sigma_{y'} - 2(\sigma_{x'} - \sigma_{y'})\cos 2\theta - 4\tau_{x'y'}\sin 2\theta + P_t + P_w,\\
&\sigma_\zeta = \sigma_{z'} - \nu\{2(\sigma_{x'} - \sigma_{y'})\cos 2\theta + 4\tau_{x'y'}\sin 2\theta - P_t\},\\
&\tau_{r\theta} = 0,\\
&\tau_{\theta\zeta} = -2\tau_{x'z'}\sin\theta + 2\tau_{y'z'}\cos\theta,\\
&\tau_{\zeta r} = 0.
\end{aligned}\right\} \quad (1)$$

where ν is Poisson's ratio. The angle θ is the angle measured from the x′ axis counter-clockwise towards the circumferential direction. The maximum tensile stress (σ_{mD}) at each point on the borehole wall and the angle (γ) between the direction perpendicular to σ_{mD} and the direction parallel to the borehole axis on the borehole wall (Fig. 2) are given by:

$$\sigma_{mD} = \frac{1}{2}\left\{\sigma_\theta + \sigma_\zeta + \sqrt{(\sigma_\theta - \sigma_\zeta)^2 + 4\tau_{\theta\zeta}{}^2}\right\}. \quad (2)$$

$$\gamma = \frac{1}{2}\tan^{-1}\left(\frac{2\tau_{\theta\zeta}}{\sigma_\theta - \sigma_\zeta}\right) \quad (3)$$

It is readily understood from equation (1) that σ_θ, σ_ζ and $\tau_{\theta\zeta}$ are periodic functions of θ with a period of 180°. Therefore, σ_{mD} given by equation (2) takes a maximum value (σ_{MD}) at the two points which are 180° apart to each other in the circumferential direction along the borehole wall.

From the above-mentioned equations, θ_{mD} and γ_m are functions of 12 parameters. Since $\sigma_{MD} = \sigma_t$ at the onset of the formation of DTF, we have the following expression from equation (2):

$$P_w = \frac{\tau_{\theta\zeta}{}^2}{\sigma_\zeta - \nu P_t - \sigma_t} + \sigma_t - P_t - \sigma_{\theta'}, \quad (4)$$

where,

$$\sigma_{\theta'} = \sigma_{x'} + \sigma_{y'} - 2(\sigma_{x'} - \sigma_{y'})\cos 2\theta - 4\tau_{x'y'}\sin 2\theta.$$

Furthermore, we know the borehole orientation at any depth , i.e., the angles φ and δ (Fig. 2). Thus, if P_t is observed and ν and σ_t are set to be appropriate values, say for example 0.25 and 0 MPa, respectively, the number of parameters can be reduced to six (number of stress components). Then the circumferential position of DTF can be calculated from the following equation:

$$\frac{d\sigma_{mD}}{d\theta} = 0. \quad (5)$$

It should be noted that the polar angle θ is the angle measured from the x′ axis on the plane normal to the borehole axis (Fig. 2) and, on the other hand, θ_{mD} is measured from y-axis (Fig. 2). Thus, θ_{mD} is given by

$$\theta_{mD} = \tan^{-1}(\cos\delta\tan\phi) + \frac{\pi}{2} - \theta_m. \quad (6)$$

where θ_m is the polar angle which satisfies equation (5).

A set of θ_{mD} and γ_m can be obtained at a depth from BHTV and/or FMI logs. If such a data set of θ_{mD} and γ_m are obtained at more than three depths where the borehole orientations are different from one another, more than six independent observation equations, with the aid of equations (3) and (5), can be set up for estimating a three-dimensional stress field. Generally speaking, geothermal and oil boreholes are drilled with deviations, and their borehole trajectories are complex. Thus, it is possible to estimate an *in situ* three-dimensional stress state from DTF data obtained in a single deviated borehole (Fig. 3), where variation of stresses with depth is needed to be constrained somehow reasonably. It is usually reasonable to suppose that the orientation of the principal axes of stress and the stress ratio are independent of depth in a depth range that is the target of estimating the stress state. From equations (2), (3), (4) and (5), the stress field is completely determined, if P_t, P_w and σ_t are given. But if P_t, P_w and σ_t are not known, only the relative stress magnitudes can be determined.

We have set up the inverse problem defined by equations (3) and (5) for the evaluation of the far-field stress state. We employ a non-linear least square method for the inversion. Instead of using the Gauss-Newton's iterative formula, here we use the Levenberg-Marquardt method for the sake of stabilizing the iteration process. The reliability of the estimated stress field is achieved by the use of a statistical approach (Okabe et al., 1998).

3. INVERSION RESULT

3.1 Method to interpret thermal stresses

Thermal stress is calculated by the following equation (Stephens and Voight, 1982).

$$P_t = \frac{\alpha E \Delta T}{1 - \nu}. \quad (7)$$

where α is a linear expansion coefficient, E Young's modulus, and ΔT is the temperature difference between mud water and rock. Table 1 shows the thermal stresses and mud water pressures which are used in the analysis. α and E are $0.3e^{-5}$ 1/℃ and 23.5 GPa respectively (referred to in the core test analysis) and they are fixed for the analysis interval. The temperature difference is calculated by the following equation, assuming the temperature difference at 930m is 100 ℃.

$$\Delta T = 100 + T_{depth} - T_{930}. \quad (8)$$

where T_{depth} is the static temperature at depth and T_{930} is the static temperature at 930m, respectively.

3.2 Inversion of DTF data obtained from borehole TG-2

Borehole TG-2 is located at Yunomori, near the Matsukawa geothermal power plant, in the Iwate prefecture in northern Japan. The borehole was kicked off at 236 m and drilled down to 1298 m in an approximate southwest direction. The maximum inclination of the hole is 38° 50' at the bottom and the open hole interval is between 710 m and 1298 m with a diameter of 8.5". The formation in the open hole interval is mainly alternating of andesite, black shale, and dacitic tuff. Both borehole televiewer (BHTV) and formation micro imager (FMI) logs were recorded. From these logs, we found DTF as shown in Fig. 1. Although we observed DTF at many depths, we selected the data taken at depths where DTF was observed clearly and both θ_{mD} and γ_m were reliable. A compilation of DTF data and their variances are shown in Table 2.

As the initial estimate for the inversion, we have chosen the stress

state obtained from the DSCA (Differential Strain Curve Analysis) core analysis at borehole TG-2. We conducted the inversion using a statistical approach under the assumption that the directions and relative magnitudes of the principal stresses do not vary with depth. Furthermore, we assumed that the Poisson's ratio (ν) was 0.25 (the averaged value of the Poisson's ratio estimated by the use of sonic logs over the depth interval of 900m to 1200m) and the tensile strength of the rock (σ_t) was 0 MPa. The inversion results are shown in Fig. 4(a). The averaged directions of the principal axes of stress are N 45.7° W ± 9.0°, 13.9° NW ± 6.0° for σ_1, N 51.0 °E ± 11.4°, 20.1° SW ± 4.6° for σ_2 and S 14.1° W ± 8.1°, 64.5° SE ± 5.2° for σ_3 and the magnitudes of σ_1, σ_2 and σ_3 are 22.7 MPa ± 1.4, 16.4 MPa ± 0.6 and 12.4 MPa ± 0.5, respectively. All three principal stresses are determined with reasonable certainty. Direction of σ_1, azimuth of σ_2 and dip of σ_3 from the results agree with the results determined without considering thermal stresses (Fig. 4). The direction of σ_1 obtained from the inversion agrees with that obtained by the stress relief method at a nearby field (Tanaka and Saito, 1980). The data θ_{mD} and γ_m calculated by using the averaged values of the stress components obtained from the inversion agreed well with the observed DTF.

4. A STUDY OF CRITICALLY STRESSED SHEAR FRCTURES BASED ON THE STRESS FIELD

Most of fractures which are shear-stressed critically are hydraulically conductive (Barton et al., 1995). We have studied critically stressed shear fractures by using the derived stress field, FMI image, BHTV image and PTS (Pressure/Temperature/Spinner) logs.

We use two coordinate systems, which are the same in section 2 to describe the shear and normal stress on each fracture (Fig. 5). If the direction cosine between the fracture plane and stress tensor are denoted by (l'_1, m'_1, n'_1), (l'_2, m'_2, n'_2) and (l'_3, m'_3, n'_3), the stress state on the fracture plane will be completely determined (Jaeger and Cook, 1969). Shear and normal stresses on the fracture plane are determined by the following equations.

$$\sigma_n = \sigma_x l_3'^2 + \sigma_y m_3'^2 + \sigma_z n_3'^2 + 2\tau_{xy} l_3' m_3' + 2\tau_{yz} m_3' n_3' + 2\tau_{zx} n_3' l_3'. \quad (9)$$

$$\tau = \sqrt{\tau_{y'z'}^2 + \tau_{z'x'}^2}. \quad (10)$$

where,

$$\tau_{y'z'} = \sigma_x l_2' l_3' + \sigma_y m_2' m_3' + \sigma_z n_2' n_3' + \tau_{xy}\left(l_2' m_3' + m_2' l_3'\right) + \tau_{yz}\left(m_2' n_3' + n_2' m_3'\right) + \tau_{yz}\left(n_2' l_3' + l_2' n_3'\right),$$

$$\tau_{z'x'} = \sigma_x l_3' l_1' + \sigma_y m_3' m_1' + \sigma_z n_3' n_1' + \tau_{xy}\left(l_3' m_1' + m_3' l_1'\right) + \tau_{yz}\left(m_3' n_1' + n_3' m_1'\right) + \tau_{yz}\left(n_3' l_1' + l_3' n_1'\right).$$

Using equations (9) and (10), shear and normal stresses are calculated for all planes of planer features picked up by the FMI logs (Fig. 6). These are expressed in a three dimensional Mohr representation (Fig. 7). The line in the figure indicates the Coulomb failure line for μ = 0.5. There are not many features stressed critically here. Most of features whose stress direction normal to the planes are orientated to σ_3 are bedding planes. Normal stress for features except bedding planes are rather large and dispersive compared with the bedding planes. Figure 8 shows PTS log while injecting the water and features at permeable zone (1070～1080m, 1130～1165m) detected by the PTS log are not so stressed critically (Fig. 9). The formation around TG-2 is not very permeable, since there was no lost circulation during drilling and the PTS was conducted under high wellhead pressure. Thus, we do not think there are many critically stressed features and we think the lost circulation occurred through bedding planes during the PTS logging. Assuming μ = 0.5, we calculated regions of critically stressed features by using a forward program. The regions are always produced between the σ_1 and σ_3 directions and the areas of the regions depend on the area limited by the Mohr's circle and Coulomb failure line. There are two critically stressed regions and their features are approximately NS～EW strike and low dip angle (Fig. 10). Interestingly, there are not any features in region "B" but there are in region "A" (Fig. 6 and Fig. 10). Six points are picked up from region "A" and the strikes of the points are calculated and compared with the faults estimated in the Matsukawa geothermal field (Fig. 11). The strikes agree with those of the three faults estimated in the field (Akazawa and Muramatsu, 1988).

5. CONCLUSIONS

Firstly, we estimated *in situ* three-dimensional stress field by using DTF (Drilling-induced Tensile Fracture) data acquired by FMI log in borehole TG-2, including thermal stresses. The data used in this analysis are four sets of circumferential positions (θ_{mD}) of DTF along the borehole surface and the inclination (γ_m) of small fractures of DTF.

Secondly, we studied critically stressed shear fractures observed in the FMI log, using the estimated stress field to investigate the feasibility of identifying permeable fractures.

The conclusions that can be drawn from the present work are summarized as follows.

1. We measured γ_m and θ_{mD} of DTF in borehole TG-2 by means of FMI log and found that the DTF data varied with depth. Four data sets were selected for the inversion. All three principal stresses are determined with reasonable certainty. Direction of σ_1, azimuth of σ_2 and dip of σ_3 from the results agree with the results determined without considering thermal stresses and the direction of σ_1 obtained from the inversion agrees with that obtained by the stress relief method at a nearby field.
2. Interpretation of the critically stressed shear fractures based on the stress field derived above shows that there are not many features stressed critically. Stress directions normal to the bedding planes are mostly orientated to σ_3 and it is possible that aperture of the bedding planes opened during the injection PTS logging.
3. Although we need further investigation to confirm the results drawn from this study, some indication of *in situ* three-dimensional stress fields, critically shear stress features and their regions around TG-2 geothermal field can be obtained.

ACKNOWLEDGEMENTS

We wish to thank NEDO (the New Energy and Industrial Technology Development Organization) for permission to publish this paper.

REFERENCES

Aadnoy, B. S. (1990). In-situ stress direction from borehole fracture traces. *J. Pet. Sci. Eng.*, Vol.4, pp.143-153.

Abé, H. and Hayashi, K. (1992). Fundamentals of design concept and design methodology for artificial geothermal reservoir systems. *Geothe. Resour. Coun. Bull.*, Vol.21, pp.149-155.

Akazawa, T. and Muramatsu, Y. (1988). Distribution of underground fractures at the Matsukawa geothermal field, northeast Japan. *J. Geother. Res. Soc. Japan*, Vol.4, pp.359-371, in Japanese with English abstract.

Barton, C. A., Zoback, M. D. and Moos, D. (1995). Fluid flow along potentially active faults in crystilline rock. *Geology*, Vol.23, pp.683-686.

Daneshy, A. A. (1973). A study of inclined hydraulic fractures. *Soc. Pet. Eng. J.*, Vol.13, pp.61-68.

Haimson, B. C. (1988). Status of in situ stress determination methods. *Proc. 29th U.S. Symp. Rock Mech.*, pp.75-84.

Hayashi, K., Shoji, T., Niitsuma, H., Ito, T. and Abé, H.

(1985). A new in situ tectonic stress measurement and its application to a geothermal model field. *Trans. Geother. Resour. Counc.*, Vol.9, pp.99-104.
Hiramatsu, Y. and Oka, Y. (1961). Stress around a shaft or level excavated in ground with a three dimensional stress state. *Mem. Fac. Eng. Kyoto Univ.*, XXIV Part 1, Vol.24, pp.56-76.
Jaeger, J. C. and Cook, N. G. W. (1969). *Fundamentals of rock mechanics.* Methuen & Co., Ltd., pp. 87-92.
Okabe, T., Hayashi, K., Shinohara, N. and Takasugi, S. (1998). Inversion of drilling-induced tensile fracture data obtained from single inclined borehole. *Int. J. Rock Mech. Min. Sci. & Geomech. Abstr.*, Vol.35, pp.747-758.
Peška, P. and Zoback, M. D. (1995). Compressive and tensile failure of inclined well bores and determination of in situ stress and rock strength. *J. Geophys. Res.*, Vol.100, pp.12791-12811.
Stephens, G. and Voight, B. (1982). Hydraulic fracturing theory for condition of thermal stress. *Int. J. Rock Mech. Min. Sci. & Geomech. Abstr.*, Vol.19, pp.279-284.
Tanaka, Y and Saito, T. (1980). Stress measurement by the stress relief method. *Gekkan Chikyu*, Vol.2, pp.630-647, in Japanese.
Yew, C. H. and Li, Y. (1988). Fracturing of a deviated well. *SPE Prod. Engineering*, pp.429-437.

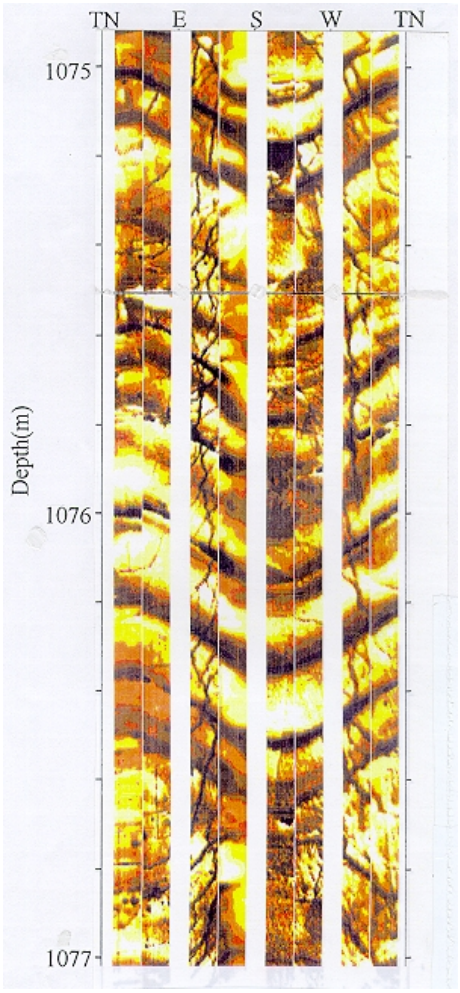

Figure 1: An electrical resistivity image (FMI image) of the borehole wall showing an en-echelon pattern of drilling-induced tensile fractures (DTF), at borehole TG-2.

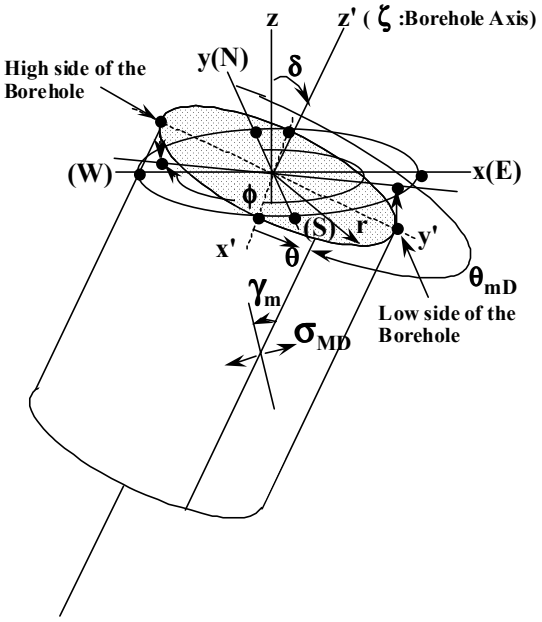

Figure 2: Illustration of the three coordinate systems and the stress state on the borehole wall.

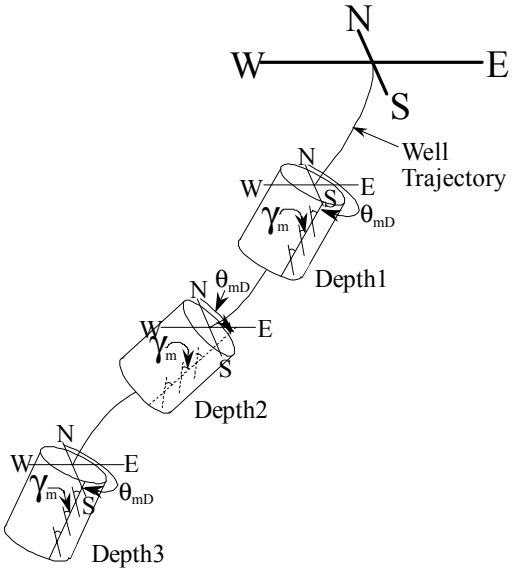

Figure 3: Conceptual representation of data sets (θ_{mD}, γ_m) for determining three-dimensional stress field.

Table 1: Thermal stresses (P_t) used in the analysis.

Depth(m)	⊿T(℃)	P_t(MPa)	P_w(MPa)
930	100	9.4	8.7
1025	116	10.9	9.5
1076	124	11.7	10.0
1192	141	13.3	10.9

Table 2: Summary of DTF data observed at borehole TG-2 and used in the present analysis.

Depth(m)	Well trajectory		θ_{mD}		γ_m	
	ϕ (deg.)	δ (deg.)	Avg.(deg.)	S.D.(deg.)	Avg.(deg.)	S.D.(deg.)
930 (890)*	214.0	27.3	114.5(6)	0.92	-24.8(6)	4.0
1025 (972)*	216.0	28.3	119.6(11)	4.0	-27.2(5)	5.0
1076 (1017)*	209.4	30.8	117.9(13)	4.1	-19.5(12)	5.3
1192 (1116)*	214.0	34.2	110.8(3)	0.75	-24.7(5)	5.4

*Vertical depth.
Avg.: Average (values in parentheses are number of samples).
S.D.: Standard Deviation.

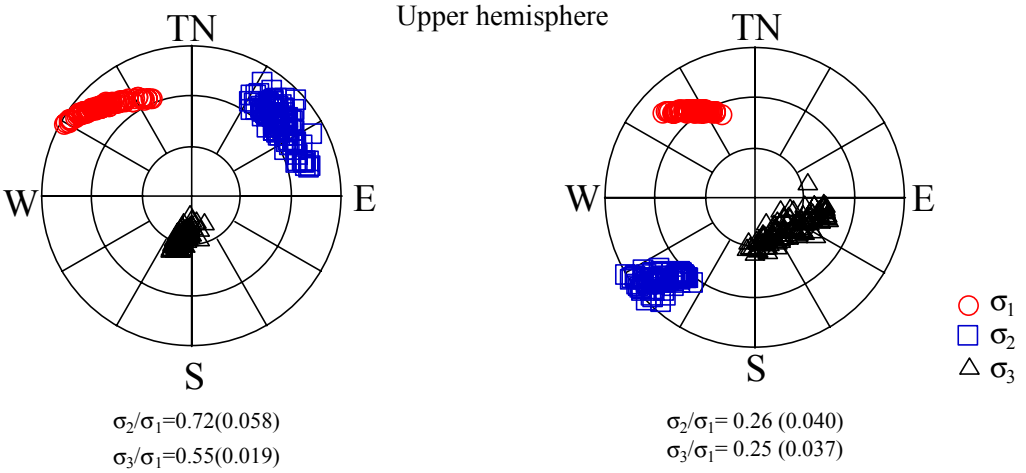

Figure 4: Inversion results, (a) considering thermal stresses,(b) without considering thermal stresses.

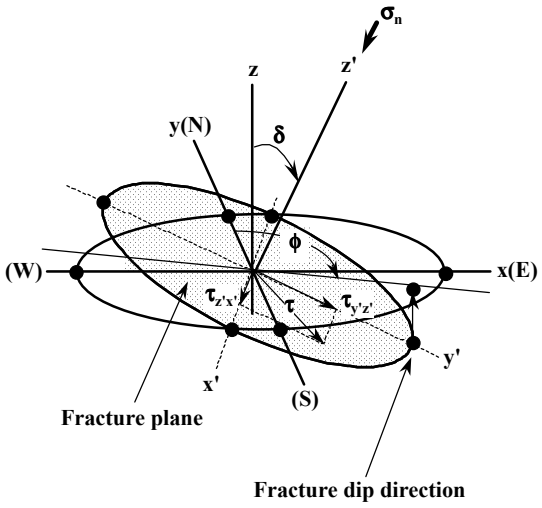

Figure 5: Coordinate systems for shear failure analysis. ϕ and δ are fracture azimuth and dip, respectively.

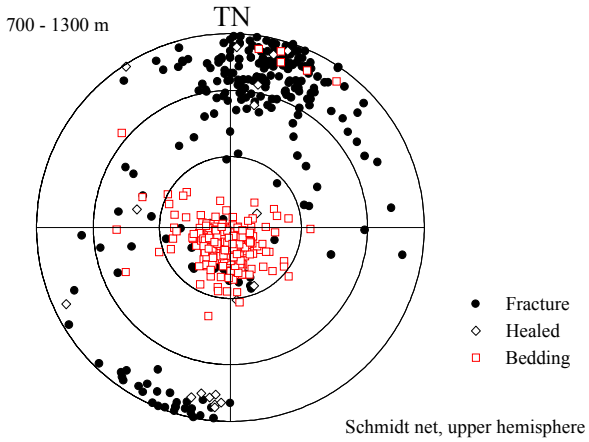

Figure 6: Poles observed by FMI log .

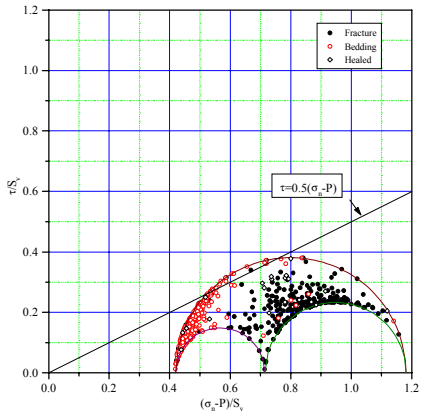

Figure 7: Normalized shear versus effective normal stress for all planer features.

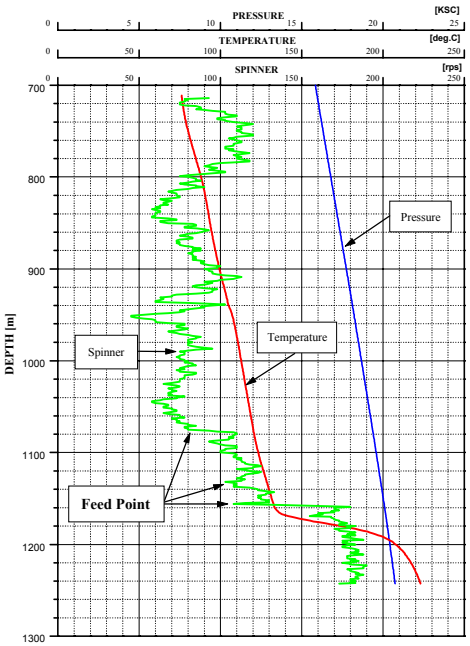

Figure 8: PTS log.

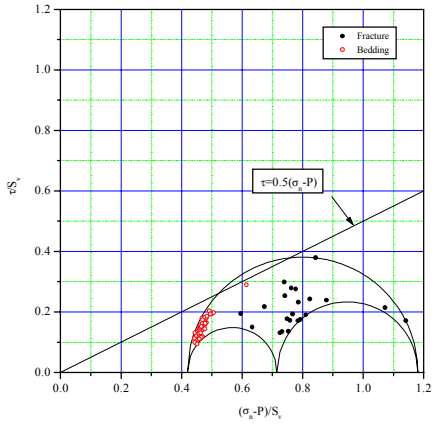

Figure 9: Normalized shear versus effective normal stress for permeable zones.

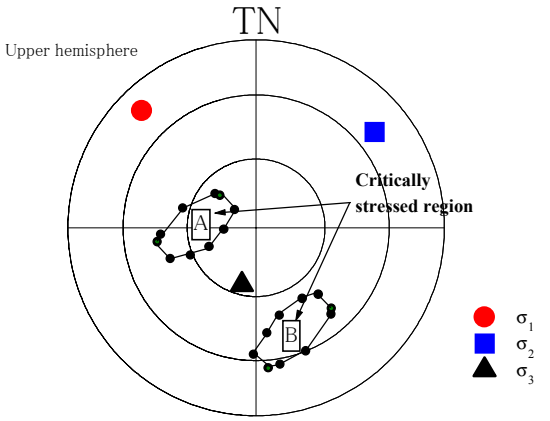

Figure 10: Relationship between critically stressed region and stress field.

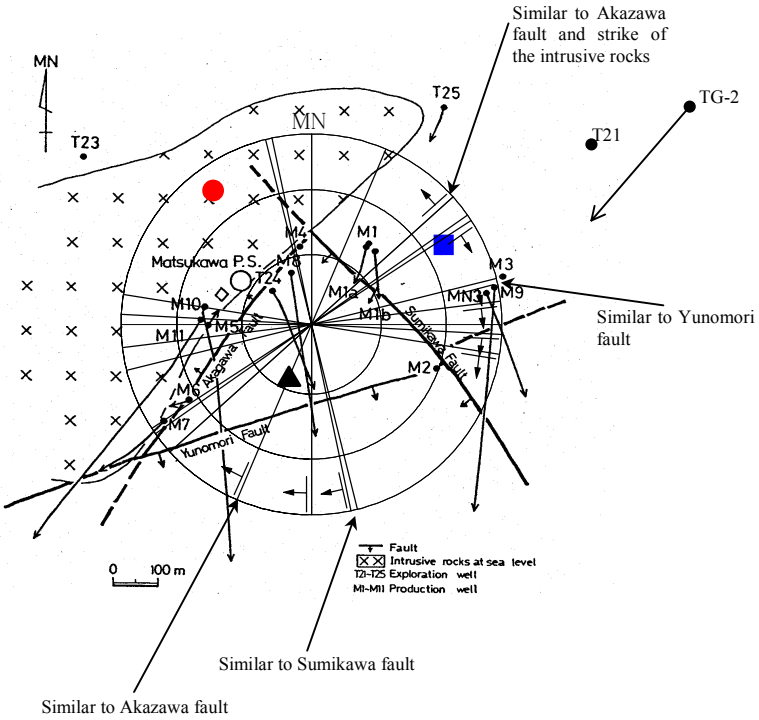

Figure 11: Comparison between strikes of critically stressed fractures and faults estimated in Matsukawa geothermal field (modified from Akazawa and Muramatsu, 1988).